Carbon quantum dots modified Bi_2WO_6 nanoflowers for enhancing photocatalytic activity: an experimental and DFT study

Kun Wu[1,2,3,4], Shaojia Song[1,2,3], Huadong Wu[1,2,3], Jia Guo[1,2,3], Linfeng Zhang[1,2,3,5] ✉

[1]*Key Laboratory for Green Chemical Process of Ministry of Education, Wuhan Institute of Technology, Wuhan 430205, People's Republic of China*
[2]*Key Laboratory of Novel Reactor and Green Chemical Technology of Hubei Province, Wuhan Institute of Technology, Wuhan 430205, People's Republic of China*
[3]*School of Chemical Engineering and Pharmacy, Wuhan Institute of Technology, Wuhan 430205, People's Republic of China*
[4]*College of Post and Telecommunications, Wuhan Institute of Technology, Wuhan 430073, People's Republic of China*
[5]*School of Chemical Engineering and Technology, Tianjin University, Tianjin 300072, People's Republic of China*
✉ *E-mail: lfzhang@wit.edu.cn*

Published in Micro & Nano Letters; Received on 9th November 2019; Revised on 16th January 2020; Accepted on 24th January 2020

Carbon quantum dots (CQDs) decorated Bi_2WO6 nanocomposites were successfully synthesised by a facile hydrothermal method. The prepared samples were characterised by the XRD, FESEM, TEM, XPS, UV–vis DRS, photocurrent and photoluminescence (PL) techniques. The DRS, photocurrent, PL spectra measurements reveal that the introduction of CQDs could broaden the absorption edge and accelerate the separation and transportation efficiency of carriers. Moreover, a reasonable charge transfer approach was given out based on the calculated work function and the differential charge difference. The CQDs/Bi_2WO_6-2 sample provides the optimal activity for photodegradation of CIP under simulated sunlight irradiation. It is hopeful that this work not only gives a reference for the design of CQDs/Bi_2WO_6 composites, but also provides some mechanistic insights into enhanced photoactivity.

1. Introduction: Human life is increasingly threatened by more and more pollutants, such as water pollutants and air pollutants [1–3]. Due to the misuse of antibiotics, antibiotic wastewater has become one of the main sources of water pollution and posed serious threats to the ecosystem [4]. Ciprofloxacin (CIP), one of the most important synthetic antibacterial agents, is widely used for treating bacterial infection. Frustratingly, not all of the CIP can be broken down by metabolism; the accumulation of CIP could induce bacterial drug resistance and subsequently pose a potential threat to both human beings and other species. Thus, the CIP pollution problem has attracted significant attention in recent years. Numerous technologies have been reported for treating wastewater, such as adsorption, photocatalysis and microwave catalysis [5–7]. The adsorption method has some fatal drawbacks like long reaction time and lower ability to degrade high concentration wastewater with high stability [5]. Microwave catalysis, as an advanced oxidation process, holds the advantage of high effectiveness. However, there still exists a big gap for large-scale applications, which was attributed to the potential risk of microwave radiation leakage [6]. The photocatalysis, as green and promising technology, has been widely studied for purifying wastewater because of its low energy consumption, simple operation and less secondary pollution [8]. The key to photocatalysis is to design efficient visible-light-driven photocatalyst. Thus, numerous photocatalysts have been designed and prepared for photocatalytic degradation, such as ZnO, C_3N_4, MOFs etc. [9–11]. Among reported photocatalysts, bismuth tungstate (Bi_2WO_6) has attracted increasing attention in virtue of its excellent performance. Firstly, its narrow bandgap (ca. 2.7 eV) could respond to visible light, which increases the utilisation of solar light [12]. Moreover, its layered structure is beneficial to facilitate the separation and transfer efficiency of photogenerated carriers. However, there still exists a lot of limits due to its inadequate reduction ability, which is determined by its relatively positive conduction band potential (ca. 0.51 eV) [13]. Thus, plenty of attempts have been carried out to improve the photocatalytic activity of Bi_2WO_6 such as controlling morphology [14], elemental doping [15] and building heterojunctions [16, 17]. Carbon materials have attracted widespread attention for designing photocatalysts due to their excellent ability to store/deliver electrons [11]. CQDs, as a novel zero-dimension carbon material, have attracted extensive interest in photocatalysis [18]. Furthermore, as illustrated by many previously reported kinds of literature, the optical property and quantum yield of CQDs could be further improved by doping modification [18, 19].

In this work, the CQDs modified Bi_2WO_6 heterostructures were synthesised by a two-step hydrothermal method. The photocatalytic performance of prepared CQDs/Bi_2WO_6 composites was evaluated by the photodegradation of CIP. The reasonable mechanism of enhanced photoactivity was presented according to the experimental properties and DFT calculation results.

2. Experimental: Firstly, the N, P co-doped CQDs solution was synthesised using sodium citrate and ammonium dihydrogen phosphate through a hydrothermal process [18]. The N, P co-doped CQDs were simplified to be CQDs in the present work. Then, the CQDs/Bi_2WO_6 composites were prepared through a hydrothermal method. Typically, 20 ml 0.05 M Na_2WO_4 CQDs-water solution (X ml CQDs solution and (20−X) ml water) was prepared. 0.98 g $Bi(NO_3)_3{\cdot}5H_2O$ was dissolved in 30 ml 0.4 M HNO_3 aqueous solution. Then, the Na_2WO_4 solution was slowly poured into the $Bi(NO_3)_3{\cdot}5H_2O$ solution. Subsequently, the mixed suspension was transferred into a 100 ml Teflon-line autoclave at 160°C for 20 h. After cooling to room temperature, the product was centrifuged and washed three times with deionised water to obtain the faint yellow powder. The prepared CQDs/Bi_2WO_6 composites were labelled as CQDs/Bi_2WO_6-1, 2, 3, 4 based on the addition of CQDs solution (0.3, 1, 3, and 5 ml), respectively. Similarly, pure Bi_2WO_6 was obtained by the same method without the addition of CQDs. The preparation process of the CQDs/Bi_2WO_6 composites is displayed in Fig. 1.

2.1. Characterisation: The crystalline phases were recorded on the D8 ADVANCE X-ray diffractometer (XRD, Bruker, Germany). The morphologies were analysed by FESEM (Zeiss Merlin

© The Institution of Engineering and Technology 2020

compact-61-78) and TEM (JEM-ARM300F) images. The XPS spectra were conducted on Escalab 250XI. The optical properties were investigated by UV–vis DRS (U-3900), photocurrent measurement (CHI 660e) and PL spectra (F-4700), respectively.

2.2. Photocatalytic activity evaluation: The activity of prepared catalysts was evaluated by the photodegradation of CIP under a 300 W Xe lamp. Typically, 40 mg photocatalysts and 200 ml CIP solution

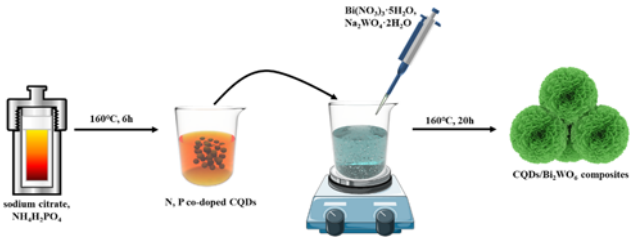


Fig. 1 *Schematic illustration of the synthesis process of CQDs/Bi_2WO_6 composites*

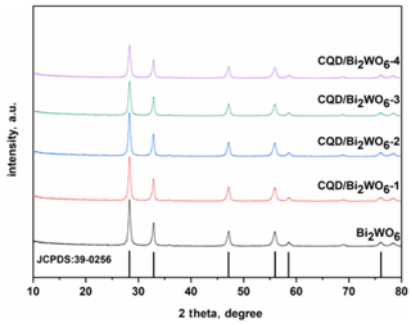


Fig. 2 *XRD patterns of the as-prepared samples*

(10 mg l^{-1}, the pH of the solution was 6.86) were added into a 350 ml quartz reactor. The reactor was placed right below the Xe lamp, and the distance between the Xe lamp and CIP solution is about 15 cm. Prior to light up, the mixture was stirred for 30 min in the dark to establish an adsorption–desorption equilibrium. At selected intervals, about 3 ml reaction mixture was collected and filtered to remove particles. The concentration of CIP was recorded on a Perkin Elmer Lambda 35 UV–vis spectrophotometer. For evaluating the visible-light photoactivity, 0.1 g tested sample was added into 100 ml 10 mg/l CIP solution, and a 300 W Xe lamp coupled with a 420 nm filter served as the light source.

3. Results and discussion: Firstly, the crystal structure of prepared samples was characterised by XRD (Fig. 2). The distinct diffraction peaks at $2\theta = 28.3°$, 32.9°, 47.1°, 56.0°, 58.5° and 76.1° could be indexed to (131), (002), (202), (133), (262) and (2102) planes of orthorhombic Bi_2WO_6 (JCPDS Card No. 39-0256), respectively. However, no characteristic diffraction peaks of CQDs can be observed, which may be due to the low CQDs content in the composite. The similar results were also reported in previous systems [18].

Fig. 3 displays the FESEM images of the prepared pure Bi_2WO_6 and CQDs/Bi_2WO_6-2 composite. All the samples show a flower-like structure and the diameters are about 4–5 µm. Furthermore, the high-resolution FESEM images clearly show that the Bi_2WO_6 microflower is constructed from a great number of nanosheets, which may promote the utilisation of light and provide more reaction substrates [20]. The CQDs/Bi_2WO_6-2 composite was further characterised by the TEM and HRTEM. As shown in Fig. 4, two different lattice fringes with d-spacings of 0.273 and 0.32 nm correspond to the (200) and (002) crystal planes of Bi_2WO_6 and graphite CQDs, respectively [2, 21].

The BET surface area, BJH pore size distribution and pore volume of pure Bi_2WO_6 and CQDs/Bi_2WO_6-2 composite are supplemented. The N_2 adsorption–desorption isotherms are shown in Fig. 5*a*, all tested samples show the typical *IV* isotherms with H3 type hysteresis. It indicates that tested catalysts hold a

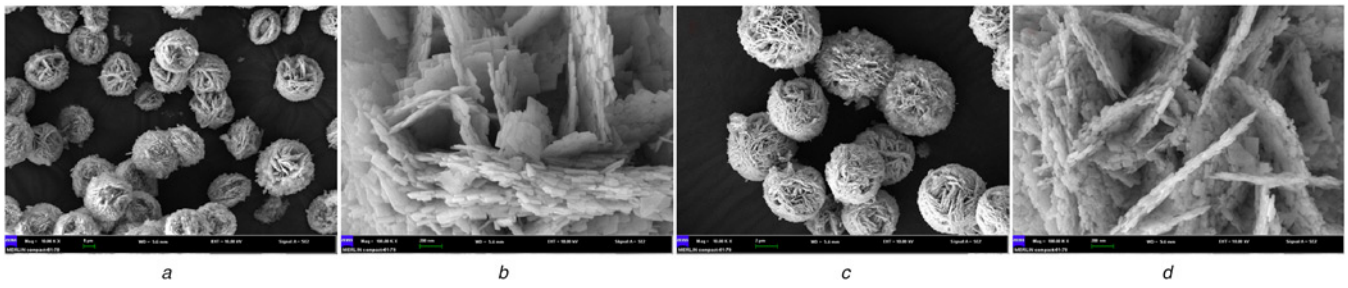


Fig. 3 *FESEM images of*
a, *b* Pure Bi_2WO_6
c, *d* CQDs/Bi_2WO_6-2 composite

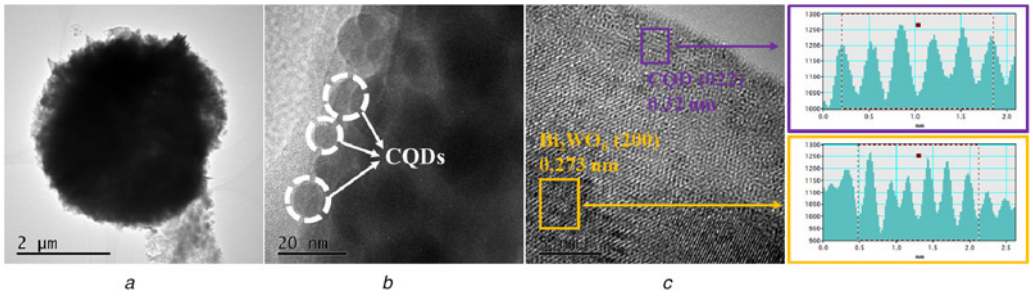


Fig. 4 *TEM and HRTEM images of the CQDs/Bi_2WO_6-2 composite*
a TEM image
b, *c* HRTEM images

© The Institution of Engineering and Technology 2020

doi: 10.1049/mnl.2019.0702

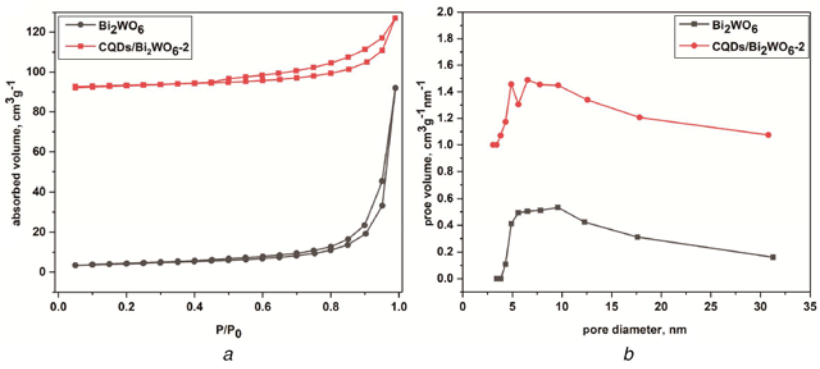


Fig. 5 *N_2 adsorption–desorption isotherms and pore structure distribution of Bi_2WO_6 and CQDs/Bi_2WO_6-2 samples*
a N_2 adsorption–desorption isotherms
b Corresponding pore size distributions of Bi_2WO_6 and CQDs/Bi_2WO_6-2

Table 1 BET surface areas and pore properties of pure Bi_2WO_6 and CQDs/Bi_2WO_6-2 composite

Sample	BET surface area, m^2g^{-1}	Average pore size, nm	Pore volume, m^3g^{-1}
Bi_2WO_6	15.03	17.358	0.141
CQDs/Bi_2WO_6-2	11.81	9.632	0.062

mesoporous structure [22]. The pore size distribution shown in Fig. 5*b* further confirms this assumption. The textural properties of tested samples are summarised in Table 1. It can be found that the BET surface area and total pore volume of CQDs/Bi_2WO_6-2 composite exhibit a decrease compared to pure Bi_2WO_6, which was mostly because the CQDs blocked the pore path of Bi_2WO_6 [23]. However, the pore size distribution did not show much difference after the decoration of CQDs, indicating that the 3D Bi_2WO_6 structure is not damaged when CQDs were combined, which was confirmed by the FESEM and TEM images.

The survey XPS spectrum (Fig. 6*a*) shows the composition of the C, N, Bi, W components, indicating the formation of CQDs and Bi_2WO_6 hybrid materials. The Bi *4f* XPS spectrum (Fig. 6*b*) shows two symmetric peaks (159.2 eV, 164.5 eV), corresponding to Bi $4f_{7/2}$ and Bi $4f_{5/2}$ signals from the Bi^{3+} species [18]. The binding energies of W $4f_{7/2}$ (35.4 eV) and W $4f_{5/2}$ (37.6 eV) can be attributed to the surface W^{6+} species. The O 1 s XPS signal (Fig. 6*d*) could be fitted into two peaks. The former peak at binding energy = 530.04 eV is assigned to the lattice oxygen species of Bi_2WO_6. While the later one at binding energy = 531.36 eV corresponds to the surface adsorbed oxygen species [24]. To confirm the presence of C, N and P elements in prepared CQDs/Bi_2WO_6-2 sample, the corresponding XPS spectrum and EDS image were performed as shown in Fig. 7. The C *1s* XPS spectrum (Fig. 7*a*) could be fitted into three peaks at 284.6, 285.8 and 288.4 eV, corresponding to the C–C, C–O and C = O bonds, respectively [25]. In addition, the binding energy located at 406.6 eV (Fig. 7*b*) could be ascribed to the N *1s* peak of nitrogen from the CQDs [26]. The EDS analysis results (Figs. 7*c* and *d*) also confirmed the coexistence of Bi, W, O, N, P elements in the CQDs/Bi_2WO_6-2 composite. It should be noted that inaccurate carbon content can be ascribed to the carbon membrane [21]. Moreover, it can also be seen that the phosphorus exists at a low level (0.37% atomic fraction). Therefore, no obvious P signal was detected in the P *2p* XPS spectrum.

The photoactivity of CQDs/Bi_2WO_6 composites was evaluated by photodegradation of CIP. As shown in Fig. 8*a*, the CQDs/Bi_2WO_6-2 exhibited the highest photocatalytic performance. Obviously, the photodegradation rate of CIP for CQDs/Bi_2WO_6-2 was estimated to be 94% after 90 min of irradiation, which was much higher than that of pure Bi_2WO_6 (58%). Subsequently, the CIP photodegradation test over CQDs/Bi_2WO_6-2 was performed under visible light irradiation to further confirm its photocatalytic performance (Fig. 8*b*). It can be seen that 0.1 g CQDs/Bi_2WO_6-2 sample could degrade 96% CIP (100 ml, 10 mg/l) within 80 min.

To illustrate the novelty of this work, Table 2 lists the degradation rate of CIP over prepared CQDs/Bi_2WO_6-2 sample in this Letter and some similar reports in recent years [27–31]. It can be concluded that the prepared Bi_2WO_6/CQDs composite shows a competitive activity for CIP photodegradation with or without filter, which indicates the novelty of this Letter.

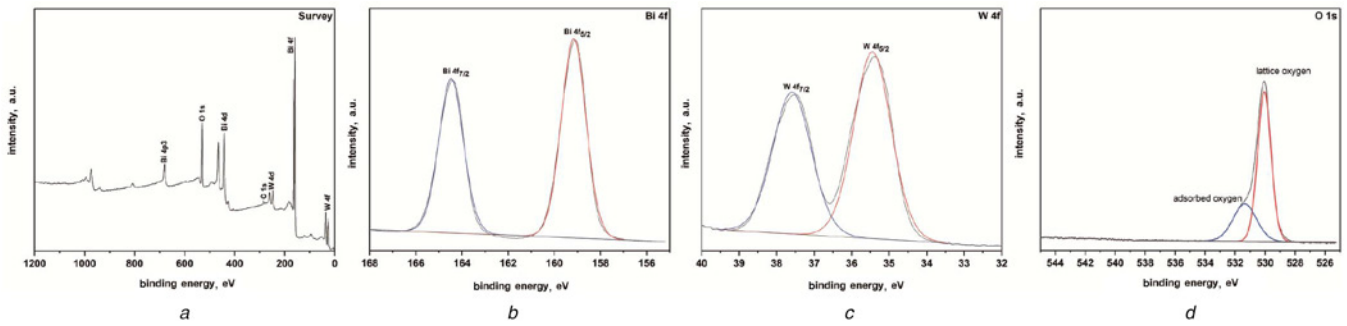


Fig. 6 *XPS spectra of CQDs/Bi_2WO_6-2 sample*
a Survey spectrum
b Bi *4f* spectrum
c W *4f* spectrum
d O *1s* spectrum

© The Institution of Engineering and Technology 2020

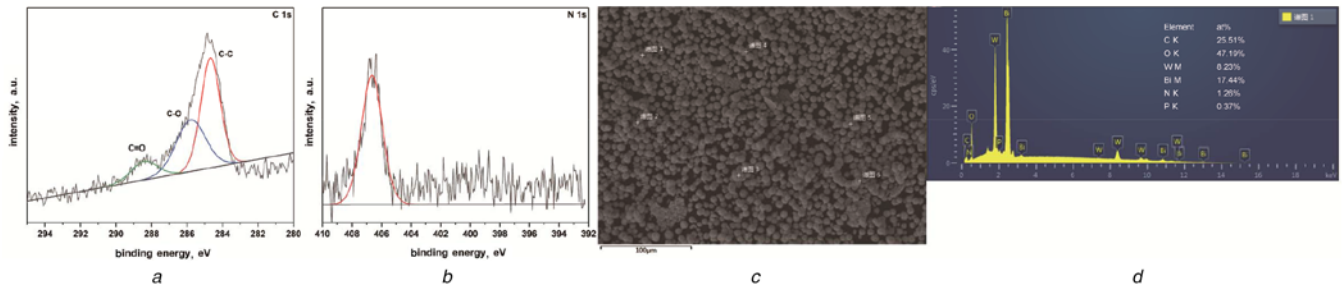


Fig. 7 *XPS spectra of CQDs/Bi_2WO_6-2 sample*
a C *1s* spectrum
b N *1s* spectrum
c, *d* EDS image of CQDs/Bi_2WO_6-2 sample

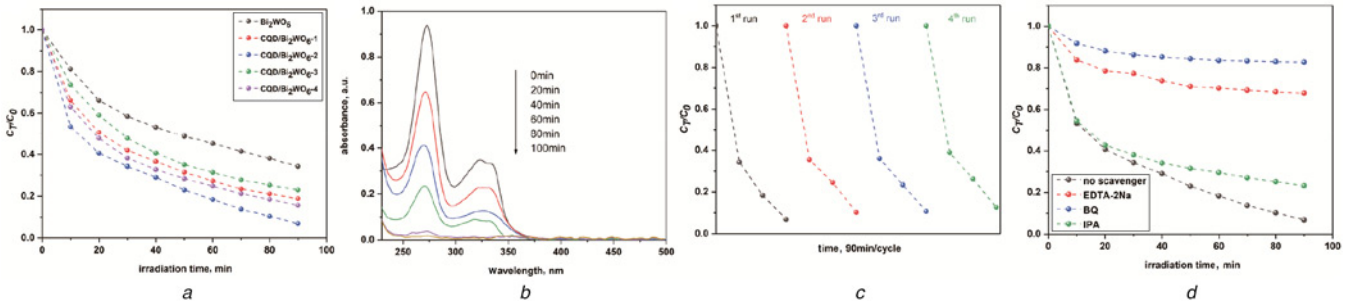


Fig. 8 *Photocatalytic performances and Scavenger experiments of prepared samples*
a Photocatalytic activity
b Visible light photoactivity over CQDs/Bi_2WO_6-2 sample
c Photocatalytic cyclability
d Scavenger experiments of prepared samples

Table 2 Comparisons of CIP photodegradation efficiency of photocatalysts in this work and similar research

Catalyst	Catalyst dosage	Light source	Removal rate	Ref.
Bi_2WO_6/RG	1 g/l	500 W Xe lamp	65%, 180 min	[27]
BiOCl@Bi_2WO_6	1 g/l	300 W Xe lamp, 420 nm filter	65%, 300 min	[28]
Bi_2WO_6/C_3N_4	1 g/l	300 W Xe lamp	20%, 120 min	[29]
Bi_2WO_6/CQDs	0.4 g/l	300 W Xe lamp, 420 nm filter	80%, 120 min	[30]
Bi_2WO_6/ BC-QDs	0.5 g/l	350 W Xe lamp, 420 nm filter	80%, 120 min	[23]
Bi_2WO_6/CQDs	0.2 g/l	300 W Xe lamp	94%, 90 min	this work
Bi_2WO_6/CQDs	1 g/l	300 W Xe lamp, 420 nm filter	96%, 80 min	this work

Moreover, the stability of photocatalyst is also a determinant for practical applications. Four cyclic experiments were conducted under the same conditions in the evaluation of photocatalytic performance. As shown in Fig. 8*c*. The CQDs/Bi_2WO_6 sample, with only a 6% decrease compared with the first run, exhibited an 87.7% CIP degradation rate for the fourth cycle. To better explore the role of active radicals in the photocatalytic reaction, the trapping experiments with different scavengers were performed [31]. As shown in Fig. 8*d*, CQDs/Bi_2WO_6 did not show obvious loss of activity when IPA was applied to trap ·OH. Nevertheless, the photoactivity was obviously limited after the addition of EDTA-2Na or BQ. The photodegradation rate of CIP decrease from 93.4 to 33% (EDTA-2Na), 18.3% (BQ), respectively. Thus, it can be deduced that h^+, $\cdot O_2^-$ are the main active radicals for the photodegradation process.

The UV–vis DRS was employed to investigate the light-response ability of samples. It is obvious that the intrinsic absorption edges showed a redshift after the introduction of CQDs, which is beneficial to improve the utilisation of the sunlight spectrum. The absorption edge of CQDs/Bi_2WO_6-2 was determined to be 451.4 nm (inset of Fig. 9*a*), and the variety of red-shift was 4.9 nm compared with that of pure Bi_2WO_6 (446.5 nm). The photocurrent (Fig. 9*b*) and PL spectra (Fig. 9*c*) were conducted to investigate the separation and transfer efficiency of charge carriers. Obviously, the CQDs/Bi_2WO_6 show a much higher photocurrent density than that of pure Bi_2WO_6, which suggests that the introduction of CQDs could suppress the recombination of photogenerated electron–hole pairs. Moreover, the PL spectrum was employed to further investigate the charge separation efficiency. As shown in Fig. 9*c*, the PL intensity decreases apparently after the CQDs have adhered to the surface of Bi_2WO_6, consistent with the photocurrent response conclusions.

In order to explore the charge transfer approach at the interface, the DFT was implemented via the CASTEP code. Firstly, the work functions of Bi_2WO_6 and CQDs were estimated to be 5.704 and 4.9 eV, respectively (here, the work function $\Phi = E_{\text{Vacuum level}} - E_{\text{Fermi level}}$). Thus, the photogenerated electrons would transfer from CQDs to Bi_2WO_6 due to the work function difference [32]. Moreover, the differential charge difference is calculated and shown in Fig. 10*c*. The electron depletion and accumulation are, respectively, labelled in red and green as shown in the right legend. Clearly, some electrons from CQDs were delocalised and flowed into Bi_2WO_6, consisting of the results of the work function.

A reasonable mechanism of the enhanced photodegradation rate of CIP is presented. The work function of Bi_2WO_6 is bigger than

© The Institution of Engineering and Technology 2020

doi: 10.1049/mnl.2019.0702

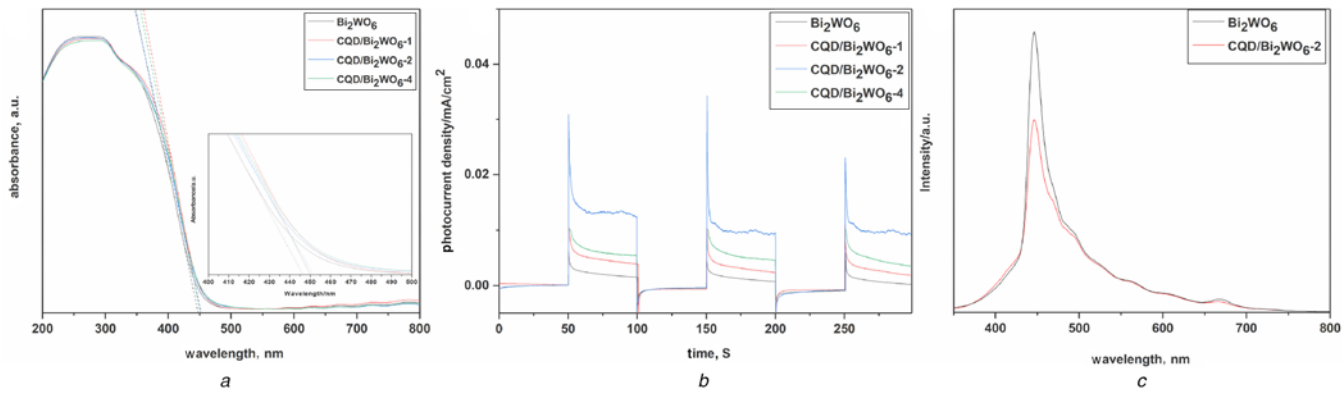


Fig. 9 *Photoelectric property characterizations of prepared samples*
a UV–vis DRS, inset: adsorption edge
b Photocurrent density
c PL spectra of samples

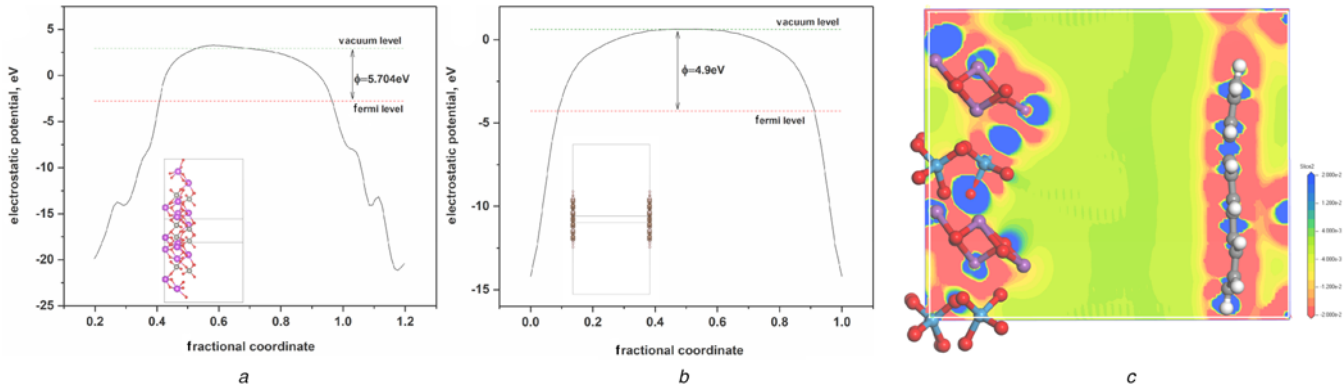


Fig. 10 *Calculated work functions*
a Bi_2WO_6 (001) plane
b CQDs (002) plane
c Charge density difference image of CQDs/Bi_2WO_6

that of CQDs. When CQDs are coated on the surface of Bi_2WO_6, the photogenerated electrons will transfer from CQDs to the Bi_2WO_6, promoting the separation and migration efficiency of charge carriers [33]. Moreover, the adsorption edge of the composites shows a red-shift due to the up-conversion property of CQDs. Benefiting from the synergistic effect of Bi_2WO_6 and CQDs, the enhanced photoactivity was obtained.

4. Conclusion: The CQDs/Bi_2WO_6 nanoflowers have been prepared and exhibited much higher photoactivity than the pure Bi_2WO_6. The introduction of CQDs can increase the visible-light absorbance, suppress the recombination of the carriers. The DFT calculations demonstrated that the electrons would flow into Bi_2WO_6 due to the differential work function. According to the quenching experiments, the $\cdot O_2^-$ and h^+ are the dominant active species in the photodegradation process. Benefiting from these advantages, the CQDs/Bi_2WO_6 composites show an enhanced photocatalytic performance for the degradation of CIP.

5. Acknowledgments: Kun Wu and Shaojia Song are contributed equally to this work and should be considered co-first authors. This project was financially supported by projects of the Scientific Research Plan Project of the Education Department of the Hubei Province [grant no. B2019377].

6 References

[1] Wang Z., Sun Q., Wang D., *ET AL.*: 'Hollow ZSM-5 zeolite encapsulated Ag nanoparticles for SO_2-resistant selective catalytic oxidation of ammonia to nitrogen', *Sep. Purif. Technol.*, 2019, **209**, pp. 1016–1026
[2] Zhang C., Zeng K., Wang C., *ET AL.*: 'LaMnO$_3$ perovskites via a facile nickel substitution strategy for boosting propane combustion performance', *Ceram. Int.*, 2020, **46**, (5), pp. 6652–6662
[3] Zhang X., Yang Y., Lv X., *ET AL.*: 'Adsorption/desorption kinetics and breakthrough of gaseous toluene for modified microporous-mesoporous UiO-66 metal organic framework', *J. Hazard. Mater.*, 2019, **366**, pp. 140–150
[4] Zou X., Yuan C., Dong Y., *ET AL.*: 'Lanthanum orthovanadate/bismuth oxybromide heterojunction for enhanced photocatalytic air purification and mechanism exploration', *Chem. Eng. J.*, 2020, **379**, p. 122380
[5] Yang Y., Ding Q., Wen D., *ET AL.*: 'Bromate removal from aqueous solution with novel flower-like Mg-Al-layered double hydroxides', *Environ. Sci. Pollut. Res.*, 2018, **25**, (27), pp. 27503–27513
[6] Zhang X., Wang Y., Hou F., *ET AL.*: 'Effects of Ag loading on structural and photocatalytic properties of flower-like ZnO microspheres', *Appl. Surf. Sci.*, 2017, **391**, pp. 476–483
[7] Wang Y., Wang Y., Yu L., *ET AL.*: 'Enhanced catalytic activity of templated-double perovskite with 3D network structure for salicylic acid degradation under microwave irradiation: insight into the catalytic mechanism', *Chem. Eng. J.*, 2019, **368**, pp. 115–128
[8] Ke J., Duan X., Luo S., *ET AL.*: 'UV-assisted construction of 3D hierarchical rGO/Bi_2MoO_6 composites for enhanced photocatalytic water oxidation', *Chem. Eng. J.*, 2017, **313**, pp. 1447–1453
[9] Zhang X., Yang Y., Huang W., *ET AL.*: 'g-C_3N_4/UiO-66 nanohybrids with enhanced photocatalytic activities for the oxidation of dye under visible light irradiation', *Mater. Res. Bull.*, 2018, **99**, pp. 349–358
[10] Li X., Pi Y., Hou Q., *ET AL.*: 'Amorphous TiO_2@NH_2-MIL-125(Ti) homologous MOF-encapsulated heterostructures with enhanced photocatalytic activity', *Chem. Commun.*, 2018, **54**, (15), pp. 1917–1920

© The Institution of Engineering and Technology 2020

[11] Yu Y., Zhu Z., Liu Z., *ET AL.*: 'Construction of the biomass carbon quantum dots modified heterojunction Bi_2WO_6/Cu_2O photocatalysis for enhancing light utilization and mechanism insight', *J. Taiwan Inst. Chem. Eng.*, 2019, **102**, pp. 197–201
[12] Phu N.D., Hoang L.H., Chen X.B., *ET AL.*: 'Study of photocatalytic activities of Bi_2WO_6 nanoparticles synthesized by fast microwave-assisted method', *J. Alloys Compd.*, 2015, **647**, pp. 123–128
[13] Zhang J., Xin J., Shao C., *ET AL.*: 'Direct Z-scheme heterostructure of p-$CuAl_2O_4$/n-Bi_2WO_6 composite nanofibers for efficient overall water splitting and photodegradation', *J. Colloid Interface Sci.*, 2019, **550**, pp. 170–179
[14] Liu W., Qu Y., Li H., *ET AL.*: 'Nanostructure Bi_2WO_6: surfactant-assisted hydrothermal synthesis for high sensitive and selective sensing of H_2S', *Sens. Actuators B, Chem.*, 2019, **294**, pp. 224–230
[15] Hoang L.H., Phu N.D., Do Chung P., *ET AL.*: 'Photocatalytic activity enhancement of Bi_2WO_6 nanoparticles by Gd-doping via microwave assisted method', *J. Mater. Sci., Mater. Electron.*, 2017, **28**, (16), pp. 12191–12196
[16] Dang Phu N., Huy Hoang L., Guo P.C., *ET AL.*: 'Study of photocatalytic activities of $Bi_2WO_6/BiVO_4$ nanocomposites', *J. Sol-Gel Sci. Technol.*, 2017, **83**, (3), pp. 640–646
[17] Lin Z., Gong J., Fu P.: 'Hierarchical Fe_2O_3/Bi_2WO_6 nanoplates with enhanced xylene sensing performance', *J. Mater. Sci., Mater. Electron.*, 2016, **28**, (5), pp. 4424–4430
[18] Song S., Wu K., Wu H., *ET AL.*: 'Multi-shelled ZnO decorated with nitrogen and phosphorus co-doped carbon quantum dots: synthesis and enhanced photodegradation activity of methylene blue in aqueous solutions', *RSC Adv.*, 2019, **9**, (13), pp. 7362–7374
[19] Lim S.Y., Shen W., Gao Z.: 'Carbon quantum dots and their applications', *Chem. Soc. Rev.*, 2015, **44**, (1), pp. 362–381
[20] Zhou H., Wen Z., Liu J., *ET AL.*: 'Z-scheme plasmonic Ag decorated WO_3/Bi_2WO_6 hybrids for enhanced photocatalytic abatement of chlorinated-VOCs under solar light irradiation', *Appl. Catal. B, Environ.*, 2019, **242**, pp. 76–84
[21] Zhang J., Yuan X., Jiang L., *ET AL.*: 'Highly efficient photocatalysis toward tetracycline of nitrogen doped carbon quantum dots sensitized bismuth tungstate based on interfacial charge transfer', *J. Colloid Interface Sci.*, 2018, **511**, pp. 296–306
[22] Zhang X., Zhang X., Song L., *ET AL.*: 'Enhanced catalytic performance for CO oxidation and preferential CO oxidation over CuO/CeO_2 catalysts synthesized from metal organic framework: effects of preparation methods', *Int. J. Hydrog. Energy*, 2018, **43**, (39), pp. 18279–18288
[23] Tang X., Yu Y., Ma C., *ET AL.*: 'The fabrication of a biomass carbon quantum dot-Bi_2WO_6 hybrid photocatalyst with high performance for antibiotic degradation', *New J. Chem.*, 2019, **43**, (47), pp. 18860–18867
[24] Zhang X., Lv X., Bi F., *ET AL.*: 'Highly efficient Mn_2O_3 catalysts derived from Mn-MOFs for toluene oxidation: the influence of MOFs precursors', *Mol. Catal.*, 2020, **482**, p. 110701
[25] Di J., Xia J., Ji M., *ET AL.*: 'The synergistic role of carbon quantum dots for the improved photocatalytic performance of Bi_2MoO_6', *Nanoscale*, 2015, **7**, (26), pp. 11433–11443
[26] Beard B.C.: 'Cellulose nitrate as a binding energy reference in N (1s) XPS studies of nitrogen-containing organic molecules', *Appl. Surf. Sci.*, 1990, **45**, (3), pp. 221–227
[27] Li Y., Chen L., Wang Y., *ET AL.*: 'Advanced nanostructured photocatalysts based on reduced graphene oxide-flower-like Bi_2WO_6 composites for an augmented simulated solar photoactivity activity', *Mater. Sci. Eng., B*, 2016, **210**, pp. 29–36
[28] Ma Y., Chen Z., Qu D., *ET AL.*: 'Synthesis of chemically bonded BiOCl@Bi_2WO_6 microspheres with exposed (020) Bi_2WO_6 facets and their enhanced photocatalytic activities under visible light irradiation', *Appl. Surf. Sci.*, 2016, **361**, pp. 63–71
[29] Chen F., Li D., Luo B., *ET AL.*: 'Two-dimensional heterojunction photocatalysts constructed by graphite-like C_3N_4 and Bi_2WO_6 nanosheets: enhanced photocatalytic activities for water purification', *J. Alloys Compd.*, 2017, **694**, pp. 193–200
[30] Zhang M., Lai C., Li B., *ET AL.*: 'Ultrathin oxygen-vacancy abundant WO_3 decorated monolayer Bi_2WO_6 nanosheet: a 2D/2D heterojunction for the degradation of Ciprofloxacin under visible and NIR light irradiation', *J. Colloid Interface Sci.*, 2019, **556**, pp. 557–567
[31] Song S., Wu K., Wu H., *ET AL.*: 'Effect of Fe/Sn doping on the photocatalytic performance of multi-shelled ZnO microspheres: experimental and theoretical investigations', *Dalton Trans.*, 2019, **48**, (35), pp. 13260–13272
[32] Tanabe I., Ozaki Y.: 'Consistent changes in electronic states and photocatalytic activities of metal (Au, Pd, Pt)-modified TiO_2 studied by far-ultraviolet spectroscopy', *Chem. Commun. (Camb)*, 2014, **50**, (17), pp. 2117–2119
[33] Wei L., Zhang H., Cao J.: 'Electrospinning of Ag/$ZnWO_4/WO_3$ composite nanofibers with high visible light photocatalytic activity', *Mater. Lett.*, 2019, **236**, pp. 171–174

© The Institution of Engineering and Technology 2020

doi: 10.1049/mnl.2019.0702